Magnetic susceptibility of a hot hadronic medium and quark degrees of freedom near the QCD crossover point

Rupam Samanta [*] and Wojciech Broniowski [†]
Institute of Nuclear Physics, Polish Academy of Sciences, 31-342 Cracow, Poland

(Received 27 November 2025; revised 11 February 2026; accepted 13 March 2026; published 6 April 2026)

The lattice QCD results for the temperature-dependent magnetic susceptibility of the medium below the crossover temperature cannot be reconciled with the widely used Hadron Resonance Gas model, also amended with the physical magnetic moments of hadrons or the pion–vector-meson loops. As noticed earlier, one observes a substantially too strong diamagnetism at temperatures in the range above ≈120 MeV compared to the lattice. This hints at a presence of quarks significantly below the QCD crossover temperature, which are needed as a source of paramagnetism. However, the pions must be retained to describe the diamagnetism data at low temperatures. Therefore, we consider here a quark-meson approach, where the temperature-dependent quark masses are fixed in a model-free way using the baryon-baryon and baryon-strangeness susceptibilities from the lattice at zero magnetic field. The constituent quarks possess anomalous magnetic moments estimated from the octet baryon magnetic moments. The vacuum quark-loop and meson-loop contributions are duly incorporated. We show that in such a framework, one can describe the magnetic susceptibility up to the crossover point. The qualitative conclusion is that the QCD degrees of freedom must extend far below the crossover temperature, down to ≈120 MeV.

DOI: 10.1103/d2gg-mgjj

I. INTRODUCTION

Magnetic properties of the hot strongly interacting medium have been actively studied on the lattice [1–14]; for recent reviews, see [15,16]. Apart from their fundamental nature, they are associated with very interesting physical phenomena, such as the chiral magnetic effect [17–19] and the magnetic catalysis and inverse catalysis (for a recent review, see, e.g., [20]), reflecting the dependence of the quark condensates on the magnetic field. The information from the lattice QCD at nonzero temperature T, vanishing chemical potentials, and nonzero magnetic field B, involves also properties such as the magnetic field dependent susceptibilities related to various conserved charges (baryon, strangeness, electric) [10,14], the chiral susceptibilities [21–23], and magnetization [7,24]. A very basic and relevant quantity is the magnetic susceptibility, χ_B [2,4,6,8,9,11], central to this work, as it describes the response of the medium to the magnetic field near $B = 0$.

It is well known that at vanishing chemical potentials QCD exhibits a crossover phase transition [25–28] near the pseudocritical temperature $T_c \approx 155$ MeV, passing gradually from the hadronic degrees of freedom below T_c to quarks and gluons above. The hadronic side is frequently described with the Hadron Resonance Gas (HRG) model [29–32], involving stable hadrons and resonances, mimicking the interhadron interactions [33,34]. HRG reproduces very well many features of the hot medium measured on the lattice [35,36]. In the absence of the magnetic field, the list includes the entropy density, the energy density and pressure, the sound velocity [37–39], the susceptibilities associated with conserved currents and their correlations, and the cumulants [40–44]. At $0 < B \lesssim 0.15$ GeV^2 (we use natural units of $\hbar = c = k_B = e = 1$ throughout this paper), the conserved charge susceptibilities [10,14,45] for $T \approx T_c$ are properly reproduced in HRG after the inclusion of the physical magnetic moments of hadrons [46].

With the above successes, HRG became a standard benchmark for the evaluation of thermodynamic quantities in the hadronic phase. Moreover, this is linked with the success in the description of the particle yields (see [47] and references therein) in ultrarelativistic nuclear collisions, where statistical hadronization with the chemical freeze-out at $T \approx T_c$ leads to a remarkable agreement of the model with the experimental data. Consequently, a common practice developed that below T_c one simply deals with just the hadrons, and above with the quarks and gluons. Certainly, the crossover nature of the transition makes the division smooth, with the hadrons and partons overlapping near T_c within some range, but a practice developed that HRG can be applied up to T_c with a high accuracy.

However, there is a notable difficulty in the application of HRG to describe the lattice data for χ_B in the region below T_c,

[*] Contact author: rupam.samanta@ifj.edu.pl
[†] Contact author: wojciech.broniowski@ifj.edu.pl

Published by the American Physical Society under the terms of the Creative Commons Attribution 4.0 International license. Further distribution of this work must maintain attribution to the author(s) and the published article's title, journal citation, and DOI. Funded by SCOAP[3].

where it works remarkably well for other observables. A comparison study was originally done in the seminal lattice papers [7,8], and more recently in [11]. In these works, diamagnetism of the QCD medium was found at T ranging from $\approx$110 MeV (lowest covered range) up to $\approx$150 MeV (the crossover temperature), fulfilling the expectations based on the fact that the pion diamagnetism dominates at low temperatures. Notably, it was a considerable qualitative improvement compared to earlier lattice QCD studies (cf. [6] and the comparison in Fig. 9 of [7]), where χ_B was not displaying diamagnetism in the covered temperature range at all. Despite the success of obtaining proper agreement between the lattice QCD and HRG at temperatures $\approx$110 MeV (where it is dominated by pions and kaons), the vivid mismatch at temperatures above $\approx$120 MeV proves that HRG is not adequate there.

In this paper, we first repeat the HRG study, showing that the mismatch persists with a complete list of hadronic states included and with physical magnetic moments of hadrons incorporated as in [46]. In a novel study, we analyze the contribution to χ_B in HRG from pion–vector-meson loops, where the resulting paramagnetic effects are small (Sec. V), at the level of 10–15%, and agree qualitatively with the two-loop Chiral Perturbation Theory [48]. We also point out that the possible effect of the hadron magnetic polarizabilities on χ_B is tiny (Sec. IV E).

We then argue, on general grounds, that to be able to describe the lattice data for χ_B above $T \approx 120$ MeV a suitable model needs to possess sufficiently *light paramagnetic* degrees of freedom that are not to be damped thermally. Natural candidates here are the quarks of constituent masses of a few hundred MeV, appearing in the thermal system from the meltdown of baryons (see, e.g., [49–51]). However, the pions must be kept, to retain the diamagnetism at lower temperatures. Hence, we apply the quark-meson framework (see [52] and references therein), which provides the needed paramagnetism in the vicinity of T_c, while pions and kaons supply diamagnetism at lower T.

The methodology applied in our analysis is as follows: we use a noninteracting quark-meson model below T_c to obtain χ_B, while demanding a simultaneous description of the lattice data for the baryon-baryon ($\chi_{\mathcal{BB}}$) and baryon-strangeness ($\chi_{\mathcal{BS}}$) susceptibilities.[1] Specifically, we use the lattice data for $\chi_{\mathcal{BB}}$ and $\chi_{\mathcal{BS}}$ (at $B = 0$) [44] to find the temperature dependence of the effective quark masses. Since these lattice studies are for $T > 135$ MeV, we are able to fix the masses above this temperature. For $\chi_{\mathcal{BB}}$, and $\chi_{\mathcal{BS}}$, as we discuss in detail in Appendix B, in the independent particle approach only the thermal part of the free energy contributes, because the vacuum part does not explicitly depend on the chemical potentials. This fact allows fixing the quark masses in a straightforward way from the thermal part of the free energy.

With the obtained temperature-dependent quark masses, and with the pions and kaons present, we compute the subtracted magnetic susceptibility $\chi_B(T) - \chi_B(0)$, as provided by the lattice simulations [8,11]. The vacuum contributions, which here are relevant [4,53], are incorporated. For the quarks, the vacuum part requires a regulator in the spirit of the low-energy effective nonperturbative models [54,55], which eliminates the contribution of the hard modes. We also investigate the relevant role of the anomalous magnetic moments of the constituent quarks.

The principal conclusion of our study is that the quark-meson model, with the vacuum terms included, complies with the lattice data for χ_B and simultaneously with $\chi_{\mathcal{BB}}$ and $\chi_{\mathcal{BS}}$, a task that has not been accomplished within HRG.

The article is organized in the following way: First, in Sec. II, we discuss the lattice results for the conserved charge susceptibilities, $\chi_{\mathcal{BB}}$ and $\chi_{\mathcal{BS}}$, as well as for the magnetic susceptibility, χ_B, comparing them to the state-of-the-art HRG calculation and pointing out the above-discussed discrepancy in the case of χ_B. We list the basic definitions of the thermodynamical framework in Sec. III. In Sec. IV, we discuss the HRG model and list the formulas for the susceptibilities in the general case with nonzero anomalous magnetic moments. Small paramagnetic pion–vector-meson loop effects are discussed in Sec. V. In Sec. VI, we incorporate the quark degrees of freedom. The results obtained within the quark-meson framework, including the necessary vacuum effects, are favorably compared to the lattice data for χ_B at temperatures from $T = 135$ MeV (the limit from the available lattice data for $\chi_{\mathcal{BB}}$ and $\chi_{\mathcal{BS}}$) up to T_c. More technical issues, in particular, the derivation of the vacuum quark-loop or the pion–vector-meson loop contributions to χ_B, are given in the Appendixes.

II. LATTICE QCD RESULTS FOR SUSCEPTIBILITIES

We begin by discussing the lattice data for the charge (baryon number and strangeness) and magnetic susceptibilities used in this work, and their comparison with the HRG model calculations. We defer the precise definitions and derivations to the following sections.

The lattice data for $\chi_{\mathcal{BB}}(T)$ and $\chi_{\mathcal{BS}}(T)$ taken from [44] are shown in Fig. 6 of Sec. VI B, and are used later in this paper (the error bars of the data are smaller than the size of the dots). The corresponding HRG results are provided in [44], as well as in other lattice references [23,41,44], pointing out a seamless agreement for temperatures all the way up to $T_c \approx 155$ MeV. Above T_c, as expected, the HRG results depart from the lattice data, as the hadronic degrees of freedom are no longer credible there.

The results for $\chi_B(T)$ are displayed in Fig. 1. We show the two most recent determinations from [8] (the photon polarization method) and [11] (the full field method), indicated with the green and orange bands, respectively. The HRG curve touches the lower-temperature (diamagnetic) end of the lattice data, where it is largely dominated by the pions, the lightest hadrons. This feature was originally brought to notice in [7], where for the first time the lattice simulations yielded a negative (diamagnetic) susceptibility at low T and exhibited compatibility with HRG for $T \lesssim 120$ MeV. This fact was confirmed later in [8,44]. As discussed in the

[1] To our knowledge, no previous quark model calculations have been able to simultaneously describe the lattice data for χ_B, $\chi_{\mathcal{BB}}$, and $\chi_{\mathcal{BS}}$.

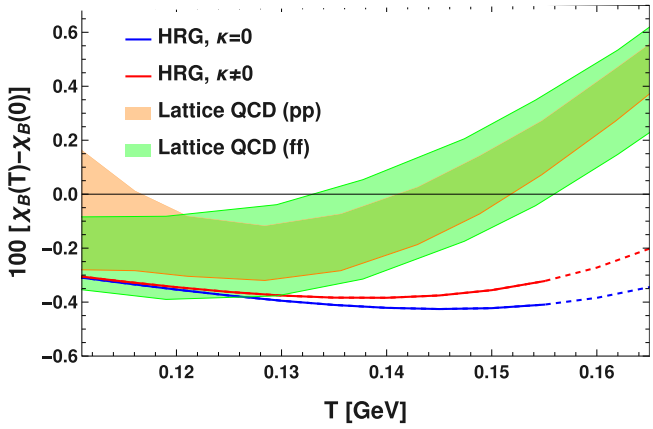


FIG. 1. Magnetic susceptibility as a function of temperature, calculated in the HRG model including (red) and excluding (blue) the anomalous magnetic moments of hadrons. The lines above T_c are dashed. The orange and green bands represent the lattice data obtained using two recent methods: the photon polarization method (pp) [8] and the full field method (ff) [11], respectively.

Introduction, the methodology applied in [8,11] improved on the earlier results (cf. [6] and the comparison in Fig. 9 in [7]), where χ_B was actually positive in the probed range of $T > 100\,\mathrm{MeV}$. Importantly, as noted in [7], for $T \gtrsim 120\,\mathrm{MeV}$, the HRG result falls noticeably below the lattice data, remaining large and negative near T_c, where the lattice χ_B crosses zero, changing the behavior from diamagnetic to paramagnetic.

Our HRG calculation is displayed in Fig. 1. In our study, we use QMHRG2020, an augmented list of hadrons including some additional quark-model states, that properly reproduces the conserved charge susceptibilities at $B = 0$ [10,44,46]. For a detailed discussion of variants of HRG, see, e.g., [56]. We also use physical magnetic moments for hadrons, as explained in [46], which induces some more paramagnetism (cf. the red and blue curves in Fig. 1) and raises the model curve by 5–10%, still falling short of the lattice data.

One should note that the lattice data shown in Fig. 1 involve a rather large extrapolation to the physical point of $m_\pi = 140\,\mathrm{MeV}$. While the mismatch between the HRG model and the lattice data displayed in Fig. 1 remains within the 2σ uncertainty, it is persistent in the wide range of $T \gtrsim 120\,\mathrm{MeV}$, indicating a genuine effect.

We also stress that χ_B, being the curvature of the pressure (the partition function) at $B = 0$ (see Sec. III), is a low-B feature. Therefore, its evaluation in the hadronic phase avoids the complications due to a possible modification of the hadronic structure and the resonances at strong B [57,58], casting doubts on the validity of HRG [59] in that case. The failure of reproducing such a basic quantity as χ_B within HRG, at temperatures where it has been traditionally used in numerous applications, urges one to rethink the composition of the hadronic medium below T_c, in search of a paramagnetic component. Moreover, the vacuum contributions, generically explicit in χ_B [4] but not treated in HRG, should be considered (see Appendix B).

III. THERMODYNAMICS IN A MAGNETIC FIELD

A. Basic definitions

Thermodynamical properties of a system treated via the grand canonical ensemble can be obtained from the grand thermodynamical potential density Ω [60,61], which in the presence of a magnetic field is

$$\Omega = U - TS - B\mathcal{M} - \mu N, \tag{1}$$

where U is the internal energy, S the entropy, $\mathcal{M}$ the magnetization, and $\mu N = \mu_{\mathcal{B}}\mathcal{B} + \mu_{\mathcal{S}}\mathcal{S} + \cdots$ involves the combination of chemical potentials and the corresponding conserved charges.[2] In the thermodynamic limit of a large volume, Ω is related to the system pressure, $P = -\Omega/V$.

The conserved charge susceptibilities used in this work are defined as

$$\chi_{\mathcal{B}\mathcal{B}} = \frac{1}{T^2}\frac{\partial^2 P}{\partial \mu_{\mathcal{B}}^2}\bigg|_{\mu_{\mathcal{B},\mathcal{S}}=0}, \quad \chi_{\mathcal{B}\mathcal{S}} = \frac{1}{T^2}\frac{\partial^2 P}{\partial \mu_{\mathcal{B}}\partial \mu_{\mathcal{S}}}\bigg|_{\mu_{\mathcal{B},\mathcal{S}}=0}. \tag{2}$$

They are evaluated at vanishing chemical potentials, as in lattice QCD.

According to Eq. (1), the magnetization density of the system is obtained as

$$\mathcal{M} = \frac{\partial \mathcal{P}}{\partial B}, \tag{3}$$

while the magnetic susceptibility is given by the second derivative of the pressure at $B = 0$,

$$\chi_B = \frac{\partial \mathcal{M}}{\partial B}\bigg|_{B=0} = \frac{\partial^2 P}{\partial B^2}\bigg|_{B=0}. \tag{4}$$

Generically, the pressure can be decomposed into the thermal and vacuum parts, $P = P^{\mathrm{th}} + P^{\mathrm{vac}}$. In the noninteracting particle picture, such as HRG or the quark-meson model studied later, at $B = 0$ the thermal part for an individual particle species (for brevity, we omit indexing of the particle species below) has the form

$$P^{\mathrm{th}} = -\eta T \sum_{s_z} \int \frac{d^3p}{(2\pi)^3} \ln[1 - \eta f(E_p, T, \mu)], \tag{5}$$

where $f(E_p, T, \mu)$ represents the occupation number of a stable hadron or a resonance with a given statistics,

$$f(E_p, T, \mu) = \frac{1}{\exp\left(\frac{E_p - \mu}{T}\right) + \eta}. \tag{6}$$

Here $E_p = \sqrt{m^2 + p^2}$ denotes the energy, s_z is the spin projection, and $\eta = +1$ or -1 depending on whether the particle is a fermion or a boson. The corresponding vacuum part can be formally written as [4]

$$P^{\mathrm{vac}} = -\frac{1}{2}\eta \sum_{s_z} \int \frac{d^3p}{(2\pi)^3} E_p, \tag{7}$$

[2]To distinguish the baryon number from the magnetic field, we use $\mathcal{B}$ for the former and B for the latter.

which is infinite and thus requires regularization, to be discussed later and detailed in Appendix C.

In the presence of a magnetic field $\vec{B} = B\hat{z}$, for charged particles the corresponding formulas involve a sum over the Landau levels l [60,61]:

$$P^{\rm th} = -\eta T \frac{B|Q|}{2\pi^2} \sum_{l=0}^{\infty} \sum_{s_z} \int_0^{\infty} dp_z \ln[1 - \eta f(p_z, B, l)],$$

$$P^{\rm vac} = -\eta \frac{B|Q|}{4\pi^2} \sum_{l=0}^{\infty} \sum_{s_z} \int_0^{\infty} dp_z E(p_z, B, l). \quad (8)$$

For the neutral particles, equations of the form of (5) and (7) hold, but E may explicitly depend on B if the particle has an anomalous magnetic moment (cf. Sec. IV A).

IV. HADRON RESONANCE GAS

A. Energy spectra

In HRG, one deals with a noninteracting system of stable hadrons and resonances, which incorporate in a simplified way the interactions between the stable hadrons [29–34,37,62].

The energy spectra of individual hadrons in a magnetic field depend on their spin. The relevant formulas were reviewed in [46]. In particular, for spin-0 charged states (e.g., $\pi^{\pm}$, $K^{\pm}$),

$$E(p_z, B, l) \equiv \epsilon_{l,p_z} = \sqrt{m^2 + p_z^2 + B|Q|(2l+1)}, \quad (9)$$

where Q denotes the particle electric charge and l labels the Landau level.

For spin-$\frac{1}{2}$ particles with an anomalous magnetic moment κ, one has the Tsai-Yildiz formula [63]

$$\epsilon_{l,p_z} = \sqrt{\left(\sqrt{m^2 + B[|Q|(2l+1) - 2Qs_z]} - 2\mu_M B\kappa s_z\right)^2 + p_z^2} \quad (10)$$

for states of nonzero charge Q (such as the proton), and

$$\epsilon_{p,p_z} = \sqrt{\left(\sqrt{m^2 + p^2 - p_z^2} - 2\mu_M B\kappa s_z\right)^2 + p_z^2} \quad (11)$$

for neutral states (such as the neutron). Here $\mu_M = \frac{1}{2m}$ is the natural magneton of the particle. Our convention for the gyromagnetic ratio of the hadron is

$$g = 2(Q + \kappa). \quad (12)$$

For higher spin states we adopt the same prescription as in [46], where the anomalous magnetic moments of hadrons are treated nonrelativistically as small corrections. For instance, in the case of spin-1 or spin-$\frac{3}{2}$ (Rarita-Schwinger) charged states [64] (e.g., ρ or Δ), we use [46]

$$\epsilon_{l,p_z} = \sqrt{m^2 + p_z^2 + B[|Q|(2l+1) - 2Qs_z]} - 2B\mu_M\kappa s_z, \quad (13)$$

and for particles with spin larger than $\frac{3}{2}$ we treat the entire spin interaction nonrelativistically [46],

$$\epsilon_{l,p_z} = \sqrt{m^2 + p_z^2 + B|Q|(2l+1)} - gB\mu_M s_z. \quad (14)$$

With the above spectra one can obtain the pressure for individual hadron species (8), which then can be used to obtain the susceptibilities. The values of κ used in the calculations presented in this paper are taken from Table I compiled in [46].

B. Baryon-baryon and baryon-strangeness susceptibilities

Using Eq. (2), one obtains a generic expression for $\chi_{Q_1Q_2}$ from the thermal part of the pressure,[3]

$$\chi_{Q_1Q_2} = \frac{Q_1Q_2(2s+1)}{2\pi^2T^2} \int_0^{\infty} dp(m^2 + 2p^2) \frac{f(E_p)}{E_p}, \quad (15)$$

where $Q_i = \mathcal{B}$ or $\mathcal{S}$, s is the particle's spin, and $f(E_p) \equiv f(E_p, T, \mu = 0)$. Summing over the particle species yields $\chi_{\mathcal{B}\mathcal{B}}$ and $\chi_{\mathcal{B}\mathcal{S}}$ in HRG, shown in Figs. 2 and 3 of [44]. The corresponding lattice data are shown in Fig. 6. In [44], it was noted that HRG is successful in describing the corresponding lattice data both qualitatively and quantitatively up to $T_c \approx 155$ MeV. Above T_c, one observes a gradual deviation, typically attributed to an emergence of the QCD degrees of freedom.

C. Magnetic susceptibility with anomalous magnetic moments

In HRG, one considers only the thermal part of the magnetic susceptibility. Some details of the straightforward derivations of the following formulas are given in Appendix A).

For the diamagnetic component one gets

$$\chi_B^{\rm dia} = -\frac{Q^2(2s+1)}{24\pi^2} \int_0^{\infty} dp \, \frac{f(E_p)}{E_p}, \quad (16)$$

which is clearly negative–definite and monotonic for each particle.

The form of the paramagnetic component depends on the spectrum used. For spin-$\frac{1}{2}$ particles with the Tsai-Yildiz expression (10), one gets (see Appendix A)

$$\chi_{B;s=\frac{1}{2}}^{\rm para} = \frac{s(s+1)(2s+1)}{6\pi^2} \int_0^{\infty} dp \times \left[Q^2 + 2Q\,\kappa + \left(1 + \frac{p^2}{m^2}\right)\kappa^2\right] \frac{f(E_p)}{E_p}. \quad (17)$$

The cases corresponding to spectra of Eqs. (13) and (14) used for higher spin states are listed in Appendix A. Obviously, all are positive-definite. In the limit of a large mass m, all the expressions reduce to the formula

$$\chi_{B;m\gg T}^{\rm para} = \frac{s(s+1)(2s+1)g^2}{24\pi^2} \int_0^{\infty} dp \frac{f(E_p)}{E_p}, \quad (18)$$

becoming proportional to the gyromagnetic factor squared. The sum $\chi_B^{\rm dia} + \chi_B^{\rm para}$ is positive for any $s > 0$ state and monotonic.

[3] It simply follows from the fact that $f(1 - \eta f) = -T df/dE_p$ and an integration by parts.

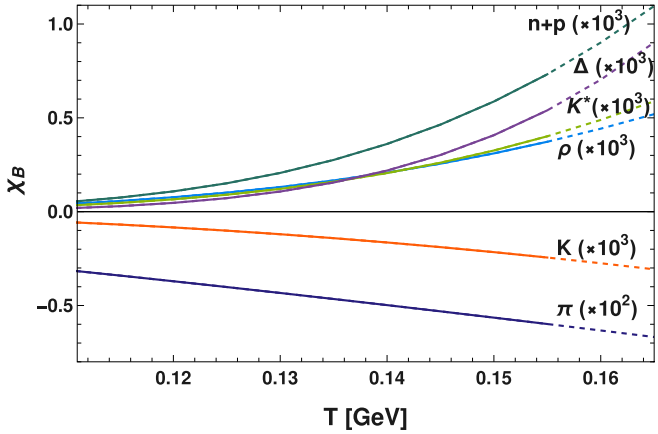


FIG. 2. Magnetic susceptibility of several hadron species as functions T with $\kappa \neq 0$. The numbers in parentheses next to labels denote factors by which a given result is multiplied (note a different factor for the pion). The hadron labels include the antiparticles and the spin-isospin degeneracy.

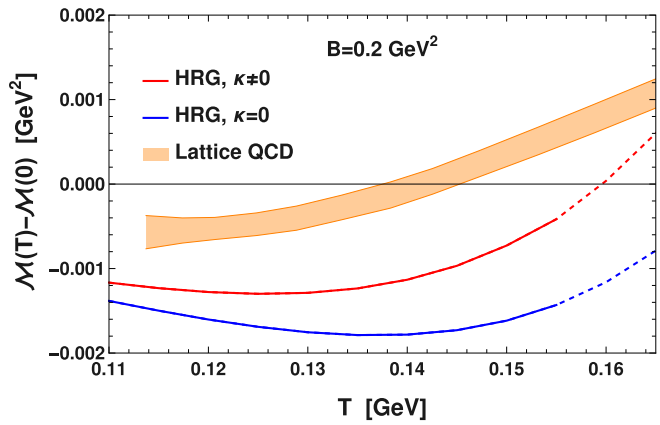


FIG. 3. Subtracted magnetization, $\mathcal{M}(B,T) - \mathcal{M}(B,0)$, at $B = 0.2$ GeV^2, plotted as a function of T. The lattice result, obtained from [7], is represented with the orange band. The blue and red curves represent, respectively, the HRG results without and with the anomalous magnetic moments of hadrons.

From the formulas for $\chi_B^{\rm para}$ it is clear that, as expected, the inclusion of the anomalous magnetic moments enhances the paramagnetic component of the magnetic susceptibility in HRG. However, with the physical κ's, the total enhancement effect is mild, as can be seen from the comparison in Fig. 1. We recall that the inclusion of the physical κ's, which are large for baryons, was crucial to achieve agreement for the conserved charge susceptibilities in HRG at nonzero values of B [46]. In Fig. 1, the HRG curves above T_c are dashed, to indicate they only carry a formal meaning there. At lower values of T, the relative effect of κ decreases, to become ≈15% of the total χ_B at $T = 140$ MeV. Hence, the mismatch between HRG results (obtained from the thermal part of the pressure) and the lattice persists even after including the anomalous magnetic moments.

D. Anatomy of the magnetic susceptibility

In order to better understand the HRG results, in Fig. 2 we show the contributions from the dominating hadron species plotted as functions of T including their anomalous magnetic moment κ. The numbers in parentheses next to the label of each curve denote a factor by which the given result is multiplied, which is 10^2 for the pion and 10^3 for the other hadrons. The result for each curve includes the corresponding antiparticles, as well as the spin and isospin (charge) degeneracy.

The magnitude of χ_B for each hadron species, naturally, grows with increasing temperature for both the paramagnetic and diamagnetic cases. It is controlled by the mass of the hadron through the occupation number via the formulas from Sec. IV C and Appendix A), which at large masses are damped approximately as $\sim e^{-M/T}$. Thus, at lower values of T higher mass hadrons are strongly suppressed and one is left with the leading diamagnetic contribution of the pion. As T increases, the kaons join the diamagnetic contribution. As a result, in the temperature range $T < 165$ MeV, the nature of HRG remains diamagnetic. At higher values of T other states appear, bringing in paramagnetic contributions, mostly from the numerous baryonic states of higher mass [65], which actually at large $T \approx 170$ MeV $> T_c$ (well outside the expected validity of HRG) prevail over the diamagnetic terms.

E. Magnetic polarizabilities of hadrons

An external constant and uniform magnetic field induces deformation of a composite object, whose dynamical response (at $T = 0$) is quantified with the magnetic polarizability. To quadratic order, the energy picks up a contribution

$$\Delta E = -\frac{1}{2}\beta B^2, \tag{19}$$

where β is the magnetic polarizability of the hadron. The estimates are $\beta_{\pi^\pm} \approx -2 \times 10^{-4}$ fm^3 [66], $\beta_{\pi^0} \approx 3 \times 10^{-4}$ fm^3[67], $\beta_n \approx 4 \times 10^{-4}$ fm^3 [68], and $\beta_p \approx 2 \times 10^{-4}$ fm^3 [68]. The term (19) in the definition of χ_B yields an extra piece for a particle species,

$$\chi_B^{\rm pol} = \frac{\beta}{2\pi^2}\int_0^\infty dp\, p^2 f(E_p), \tag{20}$$

which, as expected, is proportional to the density of states at $B = 0$. With the above-quoted values for β's, we find that $100\chi_B^{\rm pol} \approx -0.002$, negligible compared to the values of Fig. 2.

F. Magnetization

To corroborate the qualitative findings for χ_B, we also examine the magnetization $\mathcal{M}$ of Eq. (3). This quantity depends on the magnitude of the magnetic field B, which here we set to $B = 0.2$ GeV^2, sizable but not too large to avoid the problems for hadrons in a too strong magnetic field [46,57,58]. Since $\mathcal{M}$ needs subtraction due to the vacuum contribution [4], we plot this quantity subtracted at $T = 0$, namely $\mathcal{M}(B,T) - \mathcal{M}(B,0)$. Note that the possible vacuum contribution is absent in HRG, similar to the case of χ_B.

Figure 3 shows the results for the subtracted magnetization in HRG compared with lattice data [7]. We observe a feature

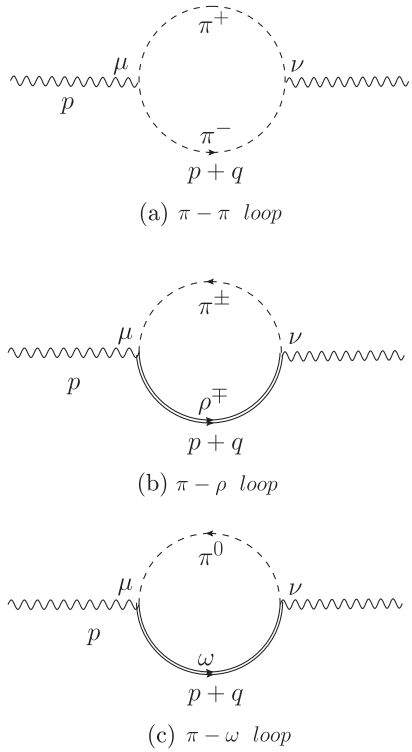


FIG. 4. Vacuum polarization diagrams for photons, involving a π loop (a) and π–vector-meson loops, (b) and (c).

qualitatively similar to that in χ_B, namely a too strong diamagnetism in HRG, placing the model curve way below the data. The effect of the anomalous magnetic moments of hadrons on $\mathcal{M}(B,T)-\mathcal{M}(B,0)$ is visible.

V. PION–VECTOR-MESON LOOPS

We now turn to yet another contribution to the paramagnetism of the medium, which originates from the pion–vector-meson loops. While such a contribution is not immediately apparent in HRG, it is manifested when considering the photon polarization in a hadronic medium, from which χ_B can be obtained. The possibility of couplings between photons, pions, and vector mesons involving the Levi-Civita tensor $\epsilon^{\alpha\beta\mu\nu}$ is well known, and such "anomalous" effects are expected to be generically small. Yet, it is worthwhile to examine the issue in more detail to have a complete hadronic picture.

According to general considerations [4,9,69,70],

$$\chi_B = \frac{1}{2}\lim_{q\to 0}\lim_{q_0\to 0}\frac{\partial^2 \mathrm{Re}[\Pi_s]}{\partial q^2}. \tag{21}$$

To pick up the thermal contribution, one calculates the vacuum polarization tensor of the photon using the loop diagrams of Fig. 4 where one of the propagators in the loop corresponds to the thermal part. For the case where both propagators in the loop correspond to the same particle, such as the pion, one obtains the formula of Eq. (16) as a check.

The loops, however, can mix different states. In particular, there is the above-mentioned coupling between a photon, pion, and a vector meson (cf. Fig. 4). A detailed calculation

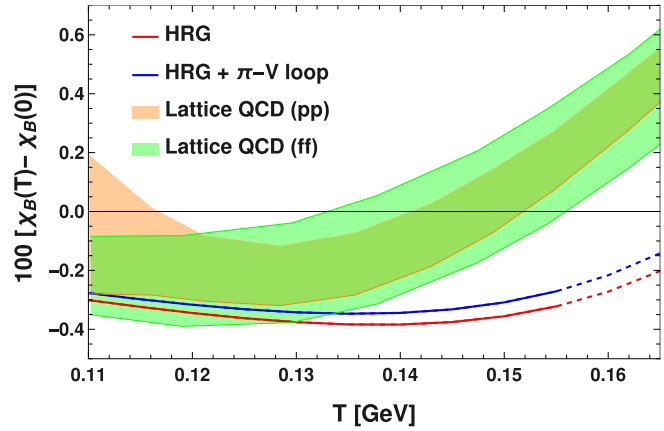


FIG. 5. Magnetic susceptibility as a function of temperature in usual HRG (red) and HRG with the contribution coming from anomalous coupling such as ρ-π and ω-π loops in the vacuum polarization of γ (blue), compared with lattice data (orange and green).

of these diagrams is provided in Appendix D 2. The magnetic susceptibility in this case becomes

$$\chi_B = -\frac{1}{12\pi^2\Delta}\left(\frac{g^2_{\gamma\pi V}}{m_V^2}\right)[I_\pi - I_V], \tag{22}$$

where $V=\rho,\omega$, $\Delta = m_V^2 - m_\pi^2$, $g_{\gamma\pi V}$ is the coupling constant, and I_a is given by

$$I_a = \int p^2 dp \frac{f(E_a)}{E_a}(p^2 - 3E_a), \quad a=\pi, V. \tag{23}$$

Here $E_a = \sqrt{p^2+m_a^2}$ represents the energy of meson a. The values of the coupling constants have been determined from the vector meson electroproduction data and have the values [71,72]

$$g_{\gamma\pi\rho} = 0.54, \quad g_{\gamma\pi\omega} = 1.82. \tag{24}$$

In Eq. (22), I_π dominates over I_V due to the small mass of the pion compared to the masses of ρ or ω.

Figure 5 shows that the contribution of the pion–vector-meson loops to χ_B is indeed small. To assess the effect, we use the HRG result from Fig. 1. It can be seen that the mixing effect is strictly paramagnetic and moderate, ranging from 10% to 20% while going from low to high temperatures. Nevertheless, it should be noted that the π-ρ contribution is larger than the ρ-ρ contribution, hence it carries some significance. Notably, the sign and the order of magnitude of the enhancement from the pion–vector-meson loops are in quantitative agreement with a two-loop chiral perturbation theory calculation [48].

VI. QUARK DEGREES OF FREEDOM

A. Motivation

In the previous sections we verified that within HRG it is not possible to achieve agreement with the lattice results for $\chi_B(T)$ in the fiducial temperature range. Even after including the anomalous magnetic moments of the hadrons or the

pion–vector-meson loops, the model remains unsuccessful in describing the lattice data. A general conclusion is that one needs sufficiently low paramagnetic states (with $s > 0$ and of sufficiently low mass), such that at $T \approx T_c$ their paramagnetism may overcome the diamagnetism from the pions and kaons. Obvious candidates here are the (constituent) quarks, which, as spin-$\frac{1}{2}$ states, are paramagnetic and light enough. Moreover, the inclusion of quarks allows one to model the needed vacuum term [4], advocated in Appendix B.

As seen from the lattice data, we also need to retain the diamagnetism at low values of T, where $\chi_B(T)$ is negative. For that reason we shall keep the pions and kaons as additional degrees of freedom, in the spirit of the quark-meson models (see [52] and references therein). Thus, we consider an independent particle model with constituent quarks of three colors and three flavors, pions, and kaons. Recently, quark meson models at nonzero B were used in similar tasks in [53,73,74].

B. Temperature-dependent quark masses from fits to $\chi_{\mathcal{BB}}$ and $\chi_{\mathcal{BS}}$

We fix the quark masses as functions of T from the requirement to describe the lattice data for $\chi_{\mathcal{BB}}$ and $\chi_{\mathcal{BS}}$ from [44] shown in panel (a) of Fig. 6. We use here Eqs. (B6) and (B7) and consider equal mass for u and d quarks, denoted by $m_l = m_u = m_d$, and an independent strange quark mass m_s. The procedure goes as follows: First, $m_s(T)$ is fitted to the $\chi_{\mathcal{BS}}$ data at each value of T according to Eq. (B7), where only the strange quarks contribute. Then, we use the obtained $m_s(T)$ to fix $m_l(T)$ with the $\chi_{\mathcal{BB}}$ data, according to Eq. (B6), where the quarks of all three flavors contribute.

The above methodology is analogous to the one from [75], where the entropy density was used to find the T dependence of constituent quarks and gluons, termed quasiparticles [76].

The obtained result for the quark masses is presented in Fig. 6. First, we note that at $T \approx T_c$ they are significantly larger than the traditional constituent masses, where $m_l \approx 300\,\mathrm{MeV}$, but, interestingly, are in the region of the quasiparticle masses of Fig. 2 in [75], where $m_l(T_c) \approx 550\,\mathrm{MeV}$ and $m_s(T_c) \approx 600\,\mathrm{MeV}$. Second, the splitting $m_s - m_l$ in our Fig. 6 is remarkably stable in the displayed range of T, being around 120–130 MeV, which is a typically expected value in the constituent quark picture.

C. Vacuum contribution

As discussed in Appendix B, the vacuum contribution to the pressure depends explicitly on B via the energy spectrum, therefore making it important for the evaluation of χ_B. In the quark-meson model, the vacuum terms were computed in [53], with dimensional regularization and renormalization applied. For the quarks, the vacuum contribution to χ_B can be evaluated according to the diagram of Fig. 7, representing the photon polarization in the quark model, $\Pi^{\mu\nu}$. We use the formula (see, e.g., [4,9,69,70])

$$\chi_B^{q,\mathrm{vac}} = \frac{1}{2}\lim_{\vec{q}\to 0}\lim_{q_0\to 0}\frac{\partial^2 \mathrm{Re}\left[\Pi_s^{q,\mathrm{vac}}\right]}{\partial q^2}, \tag{25}$$

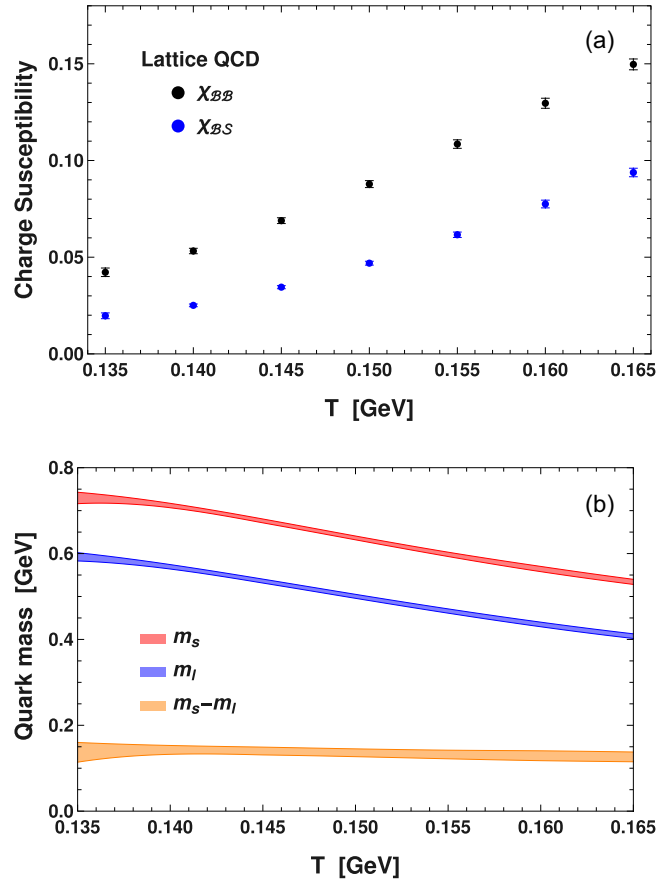


FIG. 6. (a) Lattice data [44] for susceptibilities $\chi_{\mathcal{BB}}$ (black) and $\chi_{\mathcal{BS}}$ (blue) as functions of T. (b) Light and strange quark masses as functions of T from the fit to the lattice data for $\chi_{\mathcal{BB}}$ and $\chi_{\mathcal{BS}}$ in panel (a) (the blue and red bands, respectively), and the difference $m_s - m_l$ (orange band). The width of the bands reflects the uncertainty of the lattice data.

with q_0 and $\vec{q}$ denoting the photon's momentum and $\Pi_s^{q,\mathrm{vac}} = \frac{1}{2}\sum_{i=1}^{3}\Pi_{ii}^{q,\mathrm{vac}}$.

Here, in the spirit of effective quark models, rather than carrying out the renormalization procedure, we apply a regulator and keep it to remove the hard-momentum contributions. Specifically, we use the Pauli-Villars regularization scheme with two- subtractions [54,55], as given by Eq. (C6). We also incorporate the possible anomalous magnetic moments of the constituent quarks, taking the vertex in the form [63,77–79]

$$\Gamma^\mu = Q\gamma^\mu + \frac{\kappa}{2m}\sigma^{\mu\nu}q^\nu \tag{26}$$

(see Appendix C for details).

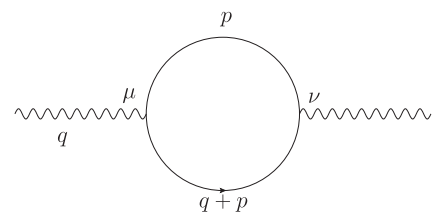


FIG. 7. Photon vacuum polarization diagram for quarks.

With the described procedure we find explicitly for each quark species (treating color separately)

$$\chi_B^{q,\mathrm{vac}}(T) = \frac{Q^2}{36\pi^2}\left(\frac{2\Lambda^4+3\Lambda^2m^2}{(\Lambda^2+m^2)^2} - 3\ln\left[\frac{\Lambda^2}{m^2}+1\right]\right) + \frac{\kappa\, Q}{4\pi^2}\left(\ln\left[\frac{\Lambda^2}{m^2}+1\right] - \frac{\Lambda^2}{\Lambda^2+m^2}\right) + \frac{\kappa^2}{48\pi^2} \times \left(\Lambda^2\left[\frac{4}{\Lambda^2+m^2} - \frac{1}{m^2}\right] - 3\ln\left[\frac{\Lambda^2}{m^2}+1\right]\right), \tag{27}$$

where $\Lambda \approx 800\,\mathrm{MeV}$ (such values are typically obtained when considering the pion structure in the vacuum [54]) is the scale of the regulator, while $m = m(T)$ is the temperature-dependent quark mass.[4]

For the mesons, one can compute the pion (or kaon) loop in the photon vacuum polarization diagram (see Fig. 4). The leading term, renormalized to 0 at $T = 0$, is [53]

$$\chi_B^{\mathrm{mes,vac}}(T) - \chi_B^{\mathrm{mes,vac}}(0) = -\frac{1}{48\pi^2}\ln\left[\frac{m(0)}{m(T)}\right], \tag{28}$$

where $m(T)$ denotes the temperature dependent pion or kaon mass. Numerous lattice and model studies suggest that these masses grow very slowly up to $\approx T_c$, where they start to increase rapidly.

D. Quark anomalous magnetic moments

The quark anomalous magnetic moments are estimated from a nonrelativistic quark model calculation of the baryon magnetic moments μ_p, μ_n, and μ_{Λ^0}, using [77,80–82]

$$\begin{aligned}\mu_p &= \tfrac{4}{3}\mu_u - \tfrac{1}{3}\mu_d,\\ \mu_n &= \tfrac{4}{3}\mu_d - \tfrac{1}{3}\mu_u,\\ \mu_\Lambda &= \mu_s.\end{aligned} \tag{29}$$

We solve the above equations with the physical values of the baryon magnetic moments (collected, e.g., in Table I of [46]). The results are $\mu_u = 1.85\ \mu_N$, $\mu_d = -0.97\ \mu_N$, and $\mu_s = -0.61\ \mu_N$, which are assumed to be independent of T. We then apply the basic equality, $\mu = gs/2m$, where s is the spin and m the mass, and using Eq. (12) we get the anomalous magnetic moments κ_q.

E. Magnetic susceptibility

The full magnetic susceptibility in the quark-meson model is

$$\chi_B(T) = N_c\sum_{u,d,s}\left[\chi_B^{\mathrm{q,th}}(T) + \chi_B^{\mathrm{q,vac}}(T)\right] + \sum_{\pi,K}\left[\chi_B^{\mathrm{mes,th}}(T) + \chi_B^{\mathrm{mes,vac}}(T)\right]. \tag{30}$$

[4]For the $\kappa = 0$ case, taking the limit $\Lambda \to \infty$ and subtracting the $T = 0$ term yields the same renormalized formula as in [53].

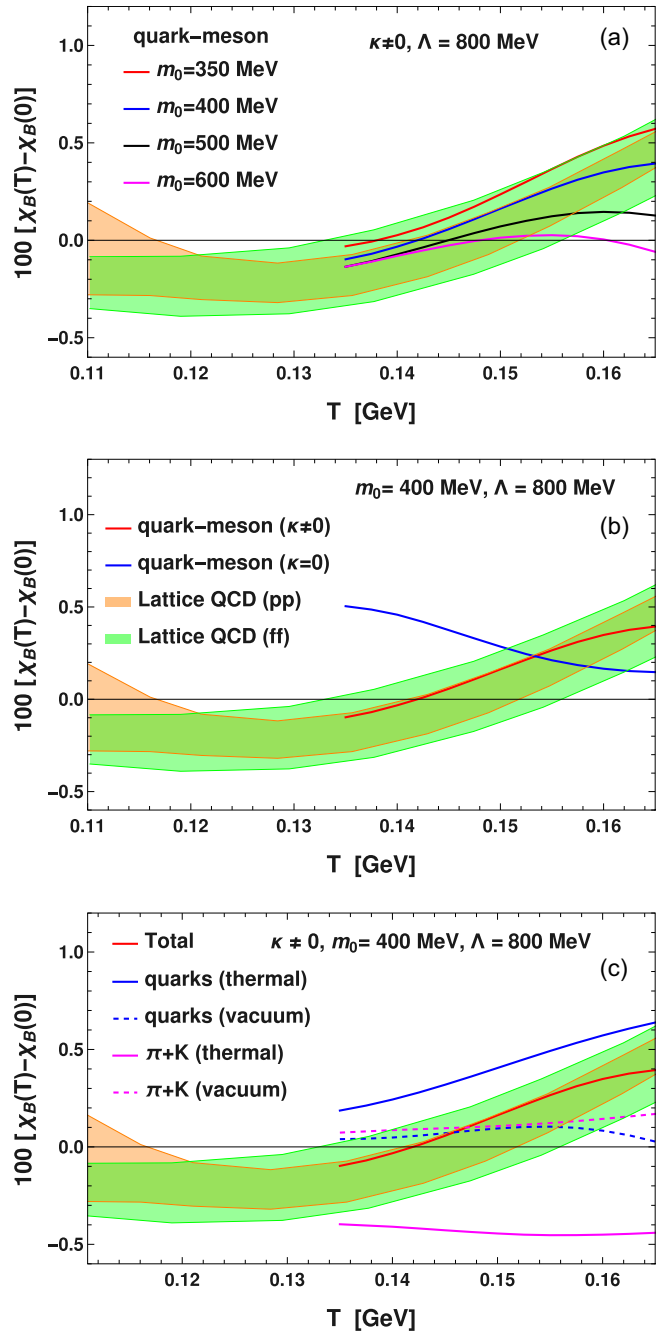


FIG. 8. (a) Magnetic susceptibility as a function of T in the quark-meson model with the fitted quark masses from Fig. 6 and the temperature dependent meson masses taken from [53]. The results include both the thermal and vacuum parts with nonzero quark anomalous magnetic moments. The results are plotted for several values of light quark masses $m_l(0) \equiv m_0$ and $m_s(0) = m_l(0) + 120\,\mathrm{MeV}$. (b) The effect of anomalous magnetic moments of the quarks in the quark-meson model. (c) Anatomy of $\chi_B(T) - \chi_B(0)$ for $m_l(0) = 400\,\mathrm{MeV}$, $\kappa_q \neq 0$, and $\Lambda = 800\,\mathrm{MeV}$.

In this formula, the quark and meson masses are temperature dependent. For the quark case, we take the dependence found in Sec. VI B in the available range of T, while for $m_\pi(T)$ and $m_K(T)$ we use the model results from the quark-meson model given in Fig. 3 of [53].

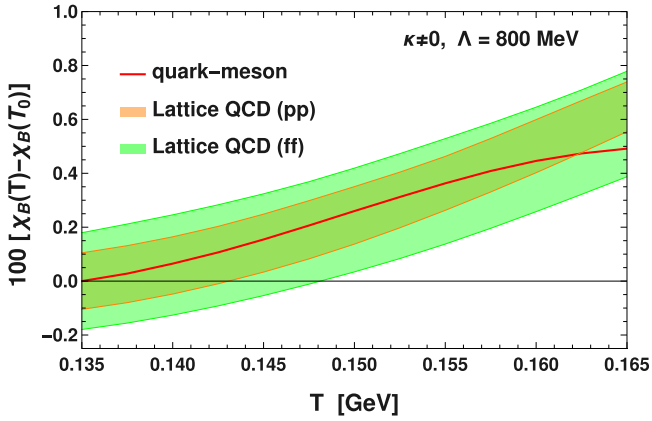


FIG. 9. Subtracted susceptibility $\chi_B(T) - \chi_B(T_0)$ with $T_0 = 135\,\mathrm{MeV}$ as a function of T. The lattice data are represented with the bands, while the red solid curve denotes the result from the quark-meson model (here independent of m_0).

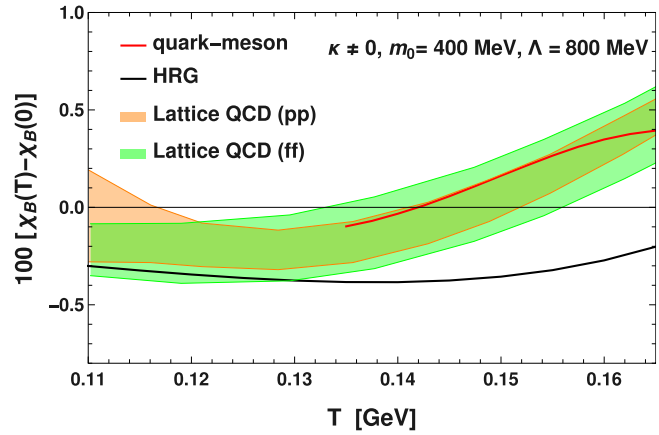


FIG. 10. Magnetic susceptibility from the quark-meson model, from HRG, and the lattice data. The HRG result includes the anomalous magnetic moments of the hadrons. The quark-meson model (with nonzero anomalous magnetic moments of the quarks) result is with $m_0 = 400\,\mathrm{MeV}$ and $\Lambda = 800\,\mathrm{MeV}$.

Since the lattice data [9,11] correspond to the subtraction $\chi_B(T) - \chi_B(0)$, we do the same in the quark meson model. The thermal parts vanish at $T = 0$, the vacuum meson part of Eq. (28) is already subtracted, whereas for the subtraction of the quark vacuum part we would need the quark masses at $T = 0$. However, these are inaccessible to the method of Sec. VI B, since the lattice data for $\chi_{\mathcal{BB}}$ and $\chi_{\mathcal{BS}}$ at $T = 0$ are not available. Thus, we first probe several reasonable values for $m_l(0)$ and $m_s(0) = m_l(0) + 120\,\mathrm{MeV}$, and later use a different subtraction scheme.

In panel (a) of Fig. 8 we present the results for $\chi_B(T) - \chi_B(0)$ obtained with the described procedure, probing several values of $m_l(0)$. All the curves start at $T = 135\,\mathrm{MeV}$, as this is the lower limit for the data of Fig. 6. We note that for the temperature range $135 < T < 155\,\mathrm{MeV}$ all the tested values of $m_l(0)$ produce a reasonable description of the lattice data within their large error band. We choose $m_l(0) = 400\,\mathrm{MeV}$ for further studies, since this value produces an acceptable agreement in Fig. 8(a), while simultaneously it is not far from estimates of the quark model in its application to the hadron structure.

In panel (b), we compare the cases with and without the quark anomalous magnetic moments, drawing the conclusion that the role of the quark anomalous magnetic moment is significant, as it largely enhances the paramagnetic component [cf. Eq. (17)].

Finally, in panel (c) we present the decomposition of $\chi_B(T) - \chi_B(0)$ into various components described in the legend. The thermal contribution for the quarks is strongly paramagnetic and increases monotonically with the temperature, while the thermal contribution of the mesons is diamagnetic and does not vary much in the considered range of T (reflecting the mild growth of the pion mass with T below T_c [53]). We stress the dominant role of the thermal part of the quarks in the monotonicity of the result.

The vacuum contribution of the quarks remains flat at low T, and above $T \approx 155\,\mathrm{MeV}$ starts to decrease, which follows from Eq. (27) with a decreasing quark mass. This falloff is responsible for the bending down of the total contribution at $T \gtrsim 155\,\mathrm{MeV}$, as seen in panels (a) and (b). The small mesonic vacuum contribution is positive and remains essentially constant for the entire temperature range with a slight increase above $T \approx 165\,\mathrm{MeV}$, where the pion mass grows.

To avoid the dependence on an unknown value of the quark mass at $T = 0$, one can subtract χ_B at a temperature within the range of the data in Fig. 6, for instance at $T_0 = 135\,\mathrm{MeV}$. We can thus obtain $\chi_B(T) - \chi_B(T_0)$ and compare it with the similarly subtracted lattice data. In Fig. 9, we show the result of such a prescription. It can be seen that the quark-meson model reproduces the lattice data very reasonably in the displayed range of temperatures.

In Fig. 10, we summarize the results of our analysis. We note that the quark-meson model with suitable parameters is able to reproduce the lattice data for χ_B in the temperature range where HRG fails.

VII. CONCLUSIONS

Here are the main results of this paper:

(1) Amending HRG with physical magnetic moment of hadrons does not cure its mismatch [7,8] with lattice data for χ_B at $T \gtrsim 120\,\mathrm{MeV}$.
(2) The contribution to χ_B from the pion–vector-meson loops is small (5–10%) and paramagnetic.
(3) The contribution of the hadronic magnetic polarizabilities to χ_B is negligible.
(4) In the quark-meson approach, it is possible to describe the lattice data for χ_B in the vicinity of the crossover point, and *simultaneously* the data for the conserved charge susceptibilities $\chi_{\mathcal{BB}}$ and $\chi_{\mathcal{BS}}$. Our modeling incorporates the vacuum contributions from the quark loops, treated with a low-energy cutoff, and from the meson loops. We have accounted for the anomalous magnetic moments of the quarks, which improve the results.

(5) The quark T-dependent masses, obtained from the precise lattice data for $\chi_{\mathcal{BB}}$ and $\chi_{\mathcal{BS}}$ from [44], are close to the quasiparticle masses of Fig. 2 in [75] but significantly larger (cf. Fig. 6) than other quark model estimates.

In general, it is clear from the lattice data that to properly model $\chi_B(T)$ one needs the pions (and kaons) to generate diamagnetism at low T [7,8] and sufficiently light fermions (quarks), yielding enough paramagnetism to raise $\chi_B(T)$ above zero beyond the crossover temperature. Our analysis shows that such a scenario is possible to realize. Moreover, we keep the agreement for $\chi_{\mathcal{BB}}$ and $\chi_{\mathcal{BS}}$ with the lattice data. More uniform quark model analyses are possible here, e.g., within the Polyakov–Nambu–Jona-Lasinio model in a magnetic field, which must be treated at the one-meson-loop level (i.e., involving the quark ring diagrams) to generate the physics of the pion loop. Such challenging studies, confronted with *all* the available lattice data, would be very interesting.

Also, with the deep implications of the lattice data for our understanding of the basics of hot media in the presence of a magnetic field, it would be very desirable to carry out future simulations leading to lower error bands in χ_B.

A final remark concerns a somewhat different topic of modeling the multiplicities in the phenomenology of ultrarelativistic heavy ion reactions, which is the key success of HRG. If the relevant degrees of freedom down to temperatures $\approx$120 MeV involve the quarks and not the baryons, as suggested by the lattice results for χ_B, then the successful application of HRG for the multiplicities should involve quark fragmentation into hadrons. Such relevant issues are left for future considerations.

ACKNOWLEDGMENT

The authors acknowledge the support from the Polish National Science Center Grant No. 2023/51/B/ST2/01625.

DATA AVAILABILITY

The data that support the findings of this article are openly available [7,8,11,44]; embargo periods may apply.

APPENDIX A: χ_B IN HRG

1. $\kappa = 0$ case

The expression for the pressure of Eq. (8) at $\kappa = 0$ becomes

$$P = \eta T \frac{B|Q|}{2\pi^2} \sum_{l=0}^{\infty} \sum_{s_z=-s}^{s} \int_0^{\infty} dp_z \times \ln\left[1+\eta \exp\left(-\frac{\sqrt{m^2+p_z^2+B[|Q|(2l+1)-2Qs_z]}}{T}\right)\right]. \tag{A1}$$

Next, applying the Euler-Mclaurin summation formula [61],

$$\sum_{l=0}^{\infty} f\left(l+\frac{1}{2}\right) \simeq \int_0^{\infty} f(x)dx + \frac{1}{24}f'(0) \tag{A2}$$

and using scaled variables $p_z = rm$, $T = tm$, and $x = z^2m^2/2B|Q|$, one obtains

$$\chi_B = \left.\frac{\partial^2 P}{\partial B^2}\right|_{B=0} = \frac{Q^2}{2\pi^2}\left(\sum_{s_z=-s}^{s} s_z^2\right) \times \int_0^{\infty} dr \times \int_0^{\infty} dz\, z \frac{[t+S(r,z)]\exp\left(\frac{S(r,z)}{t}\right)+\eta t}{t\,S(r,z)^3\left(\exp\left(\frac{S(r,z)}{t}\right)+\eta\right)^2} - \frac{Q^2}{24\pi^2}\sum_{s_z=-s}^{s}\int_0^{\infty} dr \frac{1}{S(r,0)\left(\exp\left(\frac{S(r,0)}{t}\right)+\eta\right)}, \tag{A3}$$

where $S(r,z) = \sqrt{1+r^2+z^2}$. The first term is paramagnetic (positive) and the second is diamagnetic (negative). Writing them as $\chi_B^{\rm para}$ and $\chi_B^{\rm dia}$ we obtain

$$\chi_B^{\rm dia} = -\frac{Q^2(2s+1)}{24\pi^2}\int_0^{\infty} dp \frac{f(E_p)}{E_p}, \tag{A4}$$

where $E_p = \sqrt{p^2+m^2}$ and $f(E_p)$ is the distribution function. Similarly, the paramagnetic term can be calculated by carrying out the z integration and an integration by parts,

$$\chi_B^{\rm para} = \frac{Q^2\, s(s+1)(2s+1)}{6\pi^2}\int_0^{\infty} dp\, \frac{f(E_p)}{E_p}. \tag{A5}$$

Comparing with the diamagnetic part, we have

$$\frac{\chi_B^{\rm para}}{\chi_B^{\rm dia}} = -4s(s+1), \tag{A6}$$

which for spin-$\frac{1}{2}$ states yields -3.

2. $\kappa \neq 0$ case

For the $\kappa \neq 0$ case, the diamagnetic contribution remains of course the same. The paramagnetic part depends on the spin of the particle. Let us first consider the Tsai-Yildiz formula of Eq. (10) for spin-$\frac{1}{2}$ particles. Carrying out steps similar to those in the $\kappa = 0$ case, we find the terms linear in κ,

$$\kappa \frac{Qs(s+1)(2s+1)}{3\pi^2}\int dz \int dr \times \frac{z\left(e^{\frac{S(r,z)}{t}}[-r^2t + S(0,z)^2S(r,z)] - r^2t\eta\right)}{tS(0,z)S(r,z)^3\left(e^{\frac{S(r,z)}{t}}+\eta\right)^2}, \tag{A7}$$

and quadratic in κ,

$$\kappa^2 \frac{s(s+1)(2s+1)}{6\pi^2}\int dr \int dz \times \frac{z\left[e^{\frac{S(r,z)}{t}}S(0,z)^4S(r,z) - r^2t\, S(0,z)^2\left(e^{\frac{S(r,z)}{t}}+\eta\right)\right]}{tS(0,z)^2S(r,z)^3\left(e^{\frac{S(r,z)}{t}}+\eta\right)^2}, \tag{A8}$$

which after carrying out the z integration and integration by parts over r lead to Eq. (17).

For spin-1 or $\frac{3}{2}$ particles, with Eq. (13) the paramagnetic contribution is given by

$$\chi^{\rm para}_{B;s=1,\frac{3}{2}} = \frac{s(s+1)(2s+1)}{6\pi^2}\int_0^\infty dp \times\left[Q^2+2Q\left(1+\frac{p^2}{m^2}\right)^{1/2}\kappa+\left(1+2\frac{p^2}{m^2}\right)\kappa^2\right]\frac{f(E_p)}{E_p}. \tag{A9}$$

Similarly, using the expression for higher spin particles of Eq. (14), one arrives at

$$\chi^{\rm para}_{B;s>\frac{3}{2}} = \frac{s(s+1)(2s+1)(Q+\kappa)^2}{6\pi^2} \times\int_0^\infty dp\left(1+2\frac{p^2}{m^2}\right)\frac{f(E_p)}{E_p}. \tag{A10}$$

APPENDIX B: SELF-CONSISTENCY IN QUARK MODELS

In the independent particle picture, the decomposition of the pressure into the thermal and vacuum parts involves functions of the following arguments:

$$P = P^{\rm th}(T,\mu,B;\{m\}) + P^{\rm vac}(B;\{m\}), \tag{B1}$$

where $\{m\}$ denotes the collection of quark masses. Since the energy spectrum of particles and antiparticles is the same due to the charge conjugation symmetry, we have the feature

$$P^{\rm th}(T,\mu,B;\{m\}) = P^{\rm th}(T,-\mu,B;\{m\}), \tag{B2}$$

i.e., symmetry in μ. Note that the vacuum term does not explicitly depend on the thermal parameters.

The quark masses may depend on the thermal parameters and B, namely $\{m\} = \{m(T,\mu,B)\}$, bringing additional implicit dependence in P. In effective models, P is treated as an effective potential for the determination of the quark masses (or other effective parameters, such as the value of the Polyakov loop). The self-consistency condition is

$$\frac{\partial P}{\partial m} = 0. \tag{B3}$$

Note that thus obtained mass must be a symmetric function of μ, as implied by the property (B2). In particular,

$$\partial m/\partial\mu\,|_{\mu=0} = 0. \tag{B4}$$

It is now instructive to evaluate various quantities needed in this work. The baryon density is

$$\mathcal{B} = \frac{dP}{d\mu_{\mathcal{B}}} = \frac{\partial P}{\partial\mu_{\mathcal{B}}} + \frac{\partial P}{\partial m}\frac{\partial m}{\partial\mu_{\mathcal{B}}} = \frac{\partial P^{\rm th}}{\partial\mu_{\mathcal{B}}}, \tag{B5}$$

where (B3) was used. For the susceptibility,

$$\chi_{\mathcal{B}\mathcal{B}} = \frac{1}{T^2}\frac{d^2P}{d\mu_{\mathcal{B}}^2}\bigg|_{\mu_{\mathcal{B}}=0} = \frac{1}{T^2}\bigg[\frac{\partial^2 P}{\partial\mu_{\mathcal{B}}^2} + \frac{\partial P}{\partial m}\frac{\partial^2 m}{\partial\mu_{\mathcal{B}}^2} + 2\frac{\partial^2 P}{\partial m\partial\mu_{\mathcal{B}}}\frac{\partial m}{\partial\mu_{\mathcal{B}}} + \frac{\partial^2 P}{\partial m^2}\left(\frac{\partial m}{\partial\mu_{\mathcal{B}}}\right)^2\bigg]_{\mu_{\mathcal{B}}=0} = \frac{1}{T^2}\frac{\partial^2 P^{\rm th}}{\partial\mu_{\mathcal{B}}^2}\bigg|_{\mu_{\mathcal{B}}=0}, \tag{B6}$$

where we have used conditions (B3) and (B4). An analogous equality follows for $\chi_{\mathcal{B}\mathcal{S}}$:

$$\chi_{\mathcal{B}\mathcal{S}} = \frac{1}{T^2}\frac{\partial^2 P^{\rm th}}{\partial\mu_{\mathcal{B}}\partial\mu_{\mathcal{S}}}\bigg|_{\mu_{\mathcal{B}},\mathcal{S}=0}. \tag{B7}$$

The meaning of Eqs. (B5)–(B7)) despite the simplicity of the derivation, is sound, as it allows (in the independent particle approach)one to performa "naive" evaluation of these quantities just from the thermal part. The vacuum term manifests itself only indirectly through the self-consistency conditions, in general leading to T-, μ-, or B-dependent quark masses.

For the magnetization and the magnetic susceptibility, derived using Eqs. (3) and (4), the situation is entirely different, since both the thermal and the vacuum parts depend explicitly on the magnetic field.[5] Thus, the vacuum contributes directly to $\mathcal{M}$, and χ_B and needs to be considered [4,53]. This makes the modeling of these magnetic features much more demanding, as it is a prerequisite to model the vacuum part of P.

APPENDIX C: VACUUM CONTRIBUTION TO χ_B FROM QUARK LOOPS

We consider nonzero anomalous magnetic moment of quarks. In presence of κ, the photon vacuum polarization tensor is given by

$$\Pi^{\mu\nu} = ie^2\int\frac{d^4p}{(2\pi)^4}{\rm Tr}[\Gamma^\mu S_F(p+q)\Gamma^\nu S_F(p)], \tag{C1}$$

where $\Gamma^\mu = Q\gamma^\mu + \frac{\kappa}{2m}\sigma^{\mu\nu}q^\nu$, with $\sigma^{\mu\nu} = -\frac{i}{2}[\gamma^\mu,\gamma^\nu]$. The quantities $p = (p_0,\vec{p})$ and $q = (q_0,\vec{q})$ are the loop momentum and the external momentum respectively, whereas $S_F(p)$ denotes the vacuum quark propagator,

$$S_F(p) = \frac{\not{p}+m}{p^2-m^2+i\epsilon}. \tag{C2}$$

Using Eq. (25) yields

$$\chi_B^{q,{\rm vac}} = R_0 + R_1\kappa + R_2\kappa^2, \tag{C3}$$

[5]The explicit dependence of $P^{\rm th}$ and $P^{\rm vac}$ on B originates simply from the explicit dependence of the energy spectrum on B, as discussed in detail in Sec. IV A.

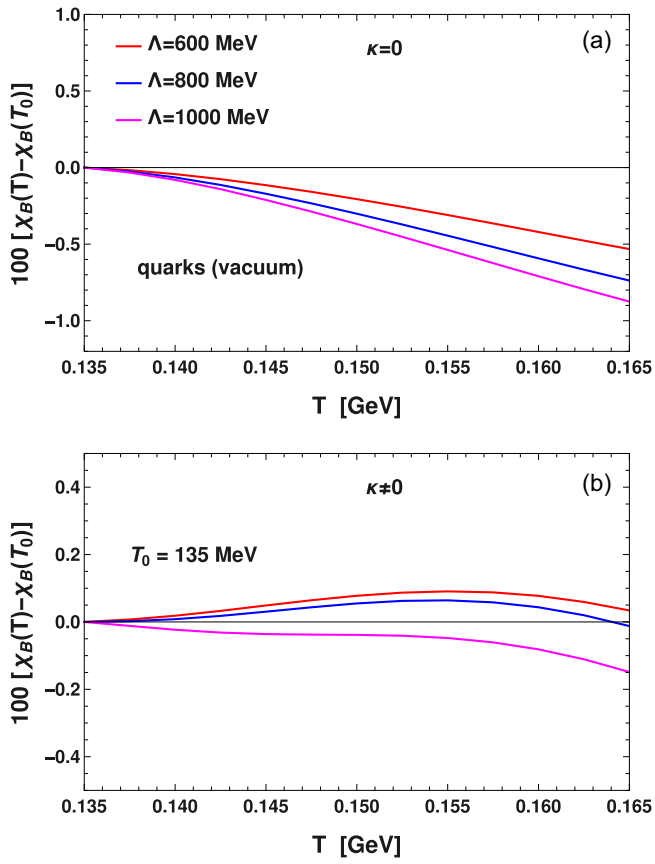


FIG. 11. Vacuum quark contribution to $\chi_B(T)$, subtracted at $T_0 = 135\,\mathrm{MeV}$, for different values of the regulator Λ, with $\kappa = 0$ (a) and $\kappa \neq 0$ (b).

where

$$R_0 = \frac{4}{3}Q^2\pi^2[(q^2+2m^2)B_0(q^2,m^2,m^2) - 2A_0(m^2)],$$
$$R_1 = 4\pi^2 Q\, q^2 B_0(q^2,m^2,m^2),$$
$$R_2 = \frac{\pi^2}{6}\frac{q^2}{M^2}[(q^2+8m^2)B_0(q^2,m^2,m^2) - 2A_0(m^2)]. \quad \text{(C4)}$$

Here A_0 and B_0 are the one-loop Passarino-Veltman (PaVe) functions [83],

$$i\pi^2 A_0(m^2) = \int d^4p\, \frac{1}{p^2-m^2+i\epsilon},\; i\pi^2 B_0(q^2,m_1^2,m_2^2) = \int d^4p \left[\frac{1}{(p+q)^2-m_1^2+i\epsilon}\frac{1}{p^2-m_2^2+i\epsilon}\right]. \quad \text{(C5)}$$

Since these integrals are divergent, one needs to use regularization. In an effective model, regularization has a meaning of suppressing the high-momentum contributions in the loop integration. Here we use Pauli-Villars regularization of [54,55] using two subtractions, amounting to the replacement of $F(\{m^2\})$ with

$$F^\Lambda(\{m^2\}) = F(\{m^2\}) - F(\{m^2+\Lambda^2\}) + \Lambda^2\frac{dF(\{M^2+\Lambda^2\})}{d\Lambda^2}, \quad \text{(C6)}$$

where F denotes a PaVe function. We explicitly obtain

$$A_0 = -\frac{m^2\ln\left(\frac{m^2}{\Lambda^2+m^2}\right)+\Lambda^2}{16\pi^4},$$
$$B_0 = \frac{\ln\left(\frac{\Lambda^2}{m^2}+1\right) - \frac{\Lambda^2}{\Lambda^2+m^2}}{16\pi^4} + \frac{\Lambda^4 q^2}{96\pi^4 m^2(\Lambda^2+m^2)^2}. \quad \text{(C7)}$$

After collecting the terms in Eq. (C3), we obtain Eq. (27).

Lattice QCD provides the results for χ_B subtracted at $T = 0$. In the absence of precise knowledge about $m(T=0)$ from our fit to the lattice data for χ_{BB} and χ_{BS}, we can subtract the value at $T_0 = 135\,\mathrm{MeV}$. The results are presented in Fig. 11 for different values of Λ, for both $\kappa = 0$ and nonzero κ. Formally, the $\Lambda \to \infty$ limit for $\kappa = 0$ reproduces the result of [4,53], which may serve as a check.

APPENDIX D: PION–VECTOR-MESON LOOP CONTRIBUTIONS TO χ_B

1. π-π loop

As a warmup, let us first consider the case where the photon vacuum polarization diagram involves a pion loop, as drawn in Fig. 4(a). The polarization tensor is

$$\Pi^{\mu\nu} = -ie^2\int\frac{d^4p}{(2\pi)^4}(2p+q)^\mu S_B(p+q)(2p+q)^\nu S_B(p), \quad \text{(D1)}$$

where the thermal propagator $S_B(p)$ is given by

$$S_B(p) = \frac{1}{p^2-m^2+i\epsilon} - 2\pi i f(|p_0|)\delta(p^2-m^2). \quad \text{(D2)}$$

Here f is the Bose-Einstein distribution function of Eq. (6).

The magnetic susceptibility is defined by Eq. (25) [9]. After plugging in the propagator in Eq. (D2) inside Eq. (D1), taking the limit $q_0 \to 0$, and carrying out the sum over the spatial index, one obtains

$$\lim_{q_0\to0}\Pi_s^{T\neq0} = -\pi e^2\int\frac{d^3p}{(2\pi)^3}\frac{dp_0}{2\pi}f(|p_0|)\delta(p_0^2-E_p^2)\times\left[\frac{q^2+4p^2+4\vec{q}\cdot\vec{p}}{p_0^2-E_p^2-q^2-2\vec{p}\cdot\vec{q}+i\epsilon} + \frac{q^2+4p^2-4\vec{q}\cdot\vec{p}}{p_0^2-E_p^2-q^2+2\vec{p}\cdot\vec{q}+i\epsilon}\right]. \quad \text{(D3)}$$

Performing the delta function integral and taking only the positive-energy contribution, one gets

$$\lim_{q_0\to0}\Pi_s^{T\neq0} = -\frac{e^2}{16\pi^2}\int p^2dp\frac{f(E_p)}{E_p}\times\int_{-1}^{+1}dz\left[\frac{q^2+4p^2+4qpz}{-q^2-2qpz+i\epsilon}+\frac{q^2+4p^2-4qpz}{-q^2+2qpz+i\epsilon}\right]. \quad \text{(D4)}$$

Keeping the real part of the above equation, carrying out the z integration, and taking the limit $\epsilon \to 0$ yields

$$\lim_{q_0\to 0} \mathrm{Re}\left[\Pi_s^{T\neq 0}\right] = \frac{e^2}{16\pi^2}\int p^2 dp \frac{f(E_p)}{E_p} \times \left[8 + \frac{q^2-4p^2}{q\,p}\ln\left(\frac{q-2p}{q+2p}\right)\right]. \quad \text{(D5)}$$

Finally, by applying Eq. (21) one arrives at Eq. (16).

Following similar methods for the fermions, one obtains Eq. (18).

2. χ_B from π–vector-meson loop

Similarly to the previous subsection, one can calculate the vacuum polarization diagram of the pion–vector-meson (π-V) loop, as drawn in Figs. 4(b) and 4(c). The only differences are the couplings at the vertices and unequal masses in the propagators, m_π and m_V. The polarization tensor in this case is given by

$$\Pi^{\mu\nu} = -ie^2\left(\frac{g^2}{m_V^2}\right)\int \frac{d^4p}{(2\pi)^4} G^{\mu\nu}(p,q) S_B^\pi(p+q) S_B^V(p), \quad \text{(D6)}$$

where

$$G^{\mu\nu}(p,q) = \varepsilon^{p\alpha q\mu}\left(\frac{p^\alpha p^\beta}{m_V^2} - g^{\alpha\beta}\right)\varepsilon^{p\beta q\nu} \quad \text{(D7)}$$

and $\varepsilon^{p\alpha q\mu} = \varepsilon_{\gamma\alpha\delta\mu}p^\gamma q^\delta$. This yields

$$\Pi_s^{T\neq 0} = -\pi e^2\left(\frac{g^2}{m_V^2}\right)\int \frac{d^4p}{(2\pi)^4} \times \left[\sum_{i=1}^{3} G^{ii}(p,q) f(|p_0|)\frac{\delta(p^2-m_V^2)}{(p+q)^2-m_\pi^2+i\epsilon} + \sum_{i=1}^{3} G^{ii}(p-q,q) f(|p_0|)\frac{\delta(p^2-m_\pi^2)}{(p-q)^2-m_V^2+i\epsilon}\right] \quad \text{(D8)}$$

and

$$\lim_{q_0\to 0}\mathrm{Re}[\Pi_s^{T\neq 0}] = -\frac{e^2}{16\pi^2}\left(\frac{g^2}{m_V^2}\right)\int p^2 dp \int_{-1}^{+1} dz \times \mathrm{Re}\left[\frac{f(E_V)}{E_V}\frac{q^2(p^2z^2-p^2+2E_V^2)}{\Delta - q^2 - 2qpz + i\epsilon} + \frac{f(E_\pi)}{E_\pi}\frac{q^2(p^2z^2-p^2+2E_\pi^2)}{-\Delta - q^2 + 2qpz + i\epsilon}\right], \quad \text{(D9)}$$

where $\Delta = m_V^2 - m_\pi^2$. Following steps similar to those in the previous subsection yields Eq. (22).

[1] G. S. Bali, F. Bruckmann, G. Endrodi, Z. Fodor, S. D. Katz, S. Krieg, A. Schafer, and K. K. Szabo, The QCD phase diagram for external magnetic fields, J. High Energy Phys. 02 (2012) 044.

[2] G. S. Bali, F. Bruckmann, M. Constantinou, M. Costa, G. Endrodi, S. D. Katz, H. Panagopoulos, and A. Schafer, Magnetic susceptibility of QCD at zero and at finite temperature from the lattice, Phys. Rev. D **86**, 094512 (2012).

[3] M. D'Elia, Lattice QCD simulations in external background fields, Lect. Notes Phys. **871**, 181 (2013).

[4] G. Endrődi, QCD equation of state at nonzero magnetic fields in the Hadron Resonance Gas model, J. High Energy Phys. 04 (2013) 023.

[5] C. Bonati, M. D'Elia, M. Mariti, F. Negro, and F. Sanfilippo, Magnetic susceptibility of strongly interacting matter across the deconfinement transition, Phys. Rev. Lett. **111**, 182001 (2013).

[6] C. Bonati, M. D'Elia, M. Mariti, F. Negro, and F. Sanfilippo, Magnetic susceptibility and equation of state of $N_f = 2+1$ QCD with physical quark masses, Phys. Rev. D **89**, 054506 (2014).

[7] G. S. Bali, F. Bruckmann, G. Endrődi, S. D. Katz, and A. Schäfer, The QCD equation of state in background magnetic fields, J. High Energy Phys. 08 (2014) 177.

[8] G. S. Bali, G. Endrődi, and S. Piemonte, Magnetic susceptibility of QCD matter and its decomposition from the lattice, J. High Energy Phys. 07 (2020) 183.

[9] G. Endrődi and G. Markó, On electric fields in hot QCD: Perturbation theory, J. High Energy Phys. 12 (2022) 015.

[10] H.-T. Ding, J.-B. Gu, A. Kumar, S.-T. Li, and J.-H. Liu, Baryon electric charge correlation as a magnetometer of QCD, Phys. Rev. Lett. **132**, 201903 (2024).

[11] B. B. Brandt, G. Endrődi, G. Markó, and A. D. M. Valois, Steady electric currents in magnetized QCD and their use for the equation of state, J. High Energy Phys. 07 (2024) 027.

[12] G. Endrődi, QCD with background electromagnetic fields on the lattice: A review, Prog. Part. Nucl. Phys. **141**, 104153 (2025).

[13] N. Astrakhantsev, V. V. Braguta, A. Y. Kotov, and A. A. Roenko, QCD equation of state at nonzero baryon density in an external magnetic field, Phys. Rev. D **109**, 094511 (2024).

[14] H.-T. Ding, J.-B. Gu, A. Kumar, and S.-T. Li, Second order fluctuations of conserved charges in external magnetic fields, Phys. Rev. D **111**, 114522 (2025).

[15] J. O. Andersen, W. R. Naylor, and A. Tranberg, Phase diagram of QCD in a magnetic field: A review, Rev. Mod. Phys. **88**, 025001 (2016).

[16] P. Adhikari, *et al.*, Strongly interacting matter in extreme magnetic fields, Prog. Part. Nucl. Phys. **146**, 104199 (2026).

[17] D. E. Kharzeev, L. D. McLerran, and H. J. Warringa, The Effects of topological charge change in heavy ion collisions: "Event by event $\mathcal{P}$ and $\mathcal{CP}$ violation", Nucl. Phys. A **803**, 227 (2008).

[18] K. Fukushima, D. E. Kharzeev, and H. J. Warringa, The chiral magnetic effect, Phys. Rev. D **78**, 074033 (2008).

[19] D. E. Kharzeev, J. Liao, S. A. Voloshin, and G. Wang, Chiral magnetic and vortical effects in high-energy nuclear collisions—A status report, Prog. Part. Nucl. Phys. **88**, 1 (2016).

[20] J. O. Andersen, QCD phase diagram in a constant magnetic background: Inverse magnetic catalysis: Where models meet the lattice, Eur. Phys. J. A **57**, 189 (2021).

[21] F. Karsch and E. Laermann, Susceptibilities, the specific heat and a cumulant in two-flavor QCD, Phys. Rev. D **50**, 6954 (1994).

[22] C. Sasaki, B. Friman, and K. Redlich, Susceptibilities and the phase structure of a chiral model with Polyakov loops, Phys. Rev. D **75**, 074013 (2007).

[23] A. Bazavov, *et al.*, The chiral and deconfinement aspects of the QCD transition, Phys. Rev. D **85**, 054503 (2012).

[24] P. Adhikari and J. O. Andersen, Quark condensates and magnetization in chiral perturbation theory in a uniform magnetic field, arXiv:2102.01080.

[25] M. A. Stephanov, K. Rajagopal, and E. V. Shuryak, Signatures of the tricritical point in QCD, Phys. Rev. Lett. **81**, 4816 (1998).

[26] Z. Fodor and S. D. Katz, Critical point of QCD at finite T and μ, lattice results for physical quark masses, J. High Energy Phys. 04 (2004) 050.

[27] Y. Aoki, G. Endrodi, Z. Fodor, S. D. Katz, and K. K. Szabo, The order of the quantum chromodynamics transition predicted by the standard model of particle physics, Nature (London) **443**, 675 (2006).

[28] K. Fukushima and T. Hatsuda, The phase diagram of dense QCD, Rep. Prog. Phys. **74**, 014001 (2011).

[29] E. Fermi, High-energy nuclear events, Prog. Theor. Phys. **5**, 570 (1950).

[30] I. Y. Pomeranchuk, On the theory of multiple particle production in a single collision, Dokl. Akad. Nauk SSSR **78**, 889 (1951).

[31] R. Hagedorn, Statistical thermodynamics of strong interactions at high-energies, Nuovo Cim. Suppl. **3**, 147 (1965).

[32] P. Koch, B. Muller, and J. Rafelski, Strangeness in relativistic heavy ion collisions, Phys. Rep. **142**, 167 (1986).

[33] R. Dashen, S.-K. Ma, and H. J. Bernstein, *S*-matrix formulation of statistical mechanics, Phys. Rev. **187**, 345 (1969).

[34] R. Venugopalan and M. Prakash, Thermal properties of interacting hadrons, Nucl. Phys. A **546**, 718 (1992).

[35] F. Karsch, K. Redlich, and A. Tawfik, Thermodynamics at nonzero baryon number density: A Comparison of lattice and hadron resonance gas model calculations, Phys. Lett. B **571**, 67 (2003).

[36] M. Gyulassy and L. McLerran, New forms of QCD matter discovered at RHIC, Nucl. Phys. A **750**, 30 (2005).

[37] P. Huovinen and P. Petreczky, QCD equation of state and hadron resonance gas, Nucl. Phys. A **837**, 26 (2010).

[38] A. Bazavov, *et al.* (HotQCD Collaboration), Equation of state in(2+1)-flavor QCD, Phys. Rev. D **90**, 094503 (2014).

[39] H.-T. Ding, F. Karsch, and S. Mukherjee, Thermodynamics of strong-interaction matter from Lattice QCD, Int. J. Mod. Phys. E **24**, 1530007 (2015).

[40] S. Borsanyi, Z. Fodor, S. D. Katz, S. Krieg, C. Ratti, and K. Szabo, Fluctuations of conserved charges at finite temperature from lattice QCD, J. High Energy Phys. 01 (2012) 138.

[41] A. Bazavov, *et al.* (HotQCD Collaboration), Fluctuations and correlations of net baryon number, electric charge, and strangeness: A comparison of lattice QCD results with the hadron resonance gas model, Phys. Rev. D **86**, 034509 (2012).

[42] R. Bellwied, S. Borsanyi, Z. Fodor, S. D. Katz, A. Pasztor, C. Ratti, and K. K. Szabo, Fluctuations and correlations in high temperature QCD, Phys. Rev. D **92**, 114505 (2015).

[43] S. Borsanyi, Z. Fodor, J. N. Guenther, S. K. Katz, K. K. Szabo, A. Pasztor, I. Portillo, and C. Ratti, Higher order fluctuations and correlations of conserved charges from lattice QCD, J. High Energy Phys. 10 (2018) 205.

[44] D. Bollweg, J. Goswami, O. Kaczmarek, F. Karsch, S. Mukherjee, P. Petreczky, C. Schmidt, and P. Scior(HotQCD Collaboration), Second order cumulants of conserved charge fluctuations revisited: Vanishing chemical potentials, Phys. Rev. D **104**, 074512 (2021).

[45] H. T. Ding, S. T. Li, Q. Shi, and X. D. Wang, Fluctuations and correlations of net baryon number, electric charge and strangeness in a background magnetic field, Eur. Phys. J. A **57**, 202 (2021).

[46] R. Samanta and W. Broniowski, Magnetic properties of the hadron resonance gas with physical magnetic moments, Phys. Rev. C **112**, 045202 (2025).

[47] A. Andronic, P. Braun-Munzinger, K. Redlich, and J. Stachel, Decoding the phase structure of QCD via particle production at high energy, Nature (London) **561**, 321 (2018).

[48] C. P. Hofmann, Diamagnetic and paramagnetic phases in low-energy quantum chromodynamics, Phys. Lett. B **818**, 136384 (2021).

[49] L. McLerran, K. Redlich, and C. Sasaki, Quarkyonic matter and chiral symmetry breaking, Nucl. Phys. A **824**, 86 (2009).

[50] L. McLerran and S. Reddy, Quarkyonic matter and neutron stars, Phys. Rev. Lett. **122**, 122701 (2019).

[51] M. Marczenko, L. McLerran, K. Redlich, and C. Sasaki, Reaching percolation and conformal limits in neutron stars, Phys. Rev. C **107**, 025802 (2023).

[52] B.-J. Schaefer and J. Wambach, The phase diagram of the quark meson model, Nucl. Phys. A **757**, 479 (2005).

[53] K. Kamikado and T. Kanazawa, Magnetic susceptibility of a strongly interacting thermal medium with 2+1 quark flavors, J. High Energy Phys. 01 (2015) 129.

[54] E. Ruiz Arriola, Pion structure at high-energies and low-energies in chiral quark models, Acta Phys. Pol. B **33**, 4443 (2002).

[55] W. Broniowski, E. Ruiz Arriola, and P. Sanchez-Puertas, Baryonic form factors of the pion and kaon in a chiral quark model, Phys. Rev. D **106**, 036001 (2022).

[56] S. Pal, Strongly interacting matter under extreme conditions, arXiv:2501.13123.

[57] M. Marczenko, M. Szymański, P. M. Lo, B. Karmakar, P. Huovinen, C. Sasaki, and K. Redlich, Magnetic effects in the hadron resonance gas, Phys. Rev. C **110**, 065203 (2024).

[58] V. Vovchenko, Magnetic field effect on hadron yield ratios and fluctuations in a hadron resonance gas, Phys. Rev. C **110**, 034914 (2024).

[59] P. Huovinen, M. Marczenko, M. Szymański, B. Karmakar, P. M. Lo, C. Sasaki, and K. Redlich, Hadron resonance gas is not a good model for hadronic matter in a strong magnetic field, in 31st International Conference on Ultra-relativistic Nucleus-Nucleus Collisions (unpublished), arXiv:2510.01431.

[60] L. D. Landau and E. M. Lifshitz, *Statistical Physics, Part 1*, Course of Theoretical Physics (Butterworth-Heinemann, Oxford, 1980), Vol. 5.

[61] R. K. Pathria and P. D. Beale, *Statistical Mechanics*, 3rd ed. (Elsevier, Amsterdam, 2011).

[62] W. Broniowski and W. Florkowski, Explanation of the RHIC $p_\perp$ spectra in a thermal model with expansion, Phys. Rev. Lett. **87**, 272302 (2001).
[63] W.-Y. Tsai and A. Yildiz, Motion of charged particles in a homogeneous magnetic field, Phys. Rev. D **4**, 3643 (1971).
[64] M. G. de Paoli, D. P. Menezes, L. B. Castro, and C. C. Barros Jr., The Rarita-Schwinger particles under the influence of strong magnetic fields, J. Phys. G: Nucl. Part. Phys. **40**, 055007 (2013).
[65] W. Broniowski, W. Florkowski, and L. Y. Glozman, Update of the Hagedorn mass spectrum, Phys. Rev. D **70**, 117503 (2004).
[66] M. Moinester, Pion polarizability 2022 status report, arXiv:2205.09954.
[67] F. He, D. B. Leinweber, A. W. Thomas, and P. Wang, Chiral extrapolation of the magnetic polarizability of the neutral pion, Phys. Rev. D **102**, 114509 (2020).
[68] S. Navas, *et al.* (Particle Data Group), Review of particle physics, Phys. Rev. D **110**, 030001 (2024).
[69] H. A. Weldon, Covariant Calculations at Finite Temperature: The Relativistic Plasma, Phys. Rev. D **26**, 1394 (1982).
[70] Y. Fujimoto and H. Yamada, A supplementary remark on finite temperature perturbation, Z. Phys. C **37**, 265 (1988).
[71] Y.-S. Oh, A. I. Titov, and T. S. H. Lee, Electromagnetic production of vector mesons at low-energies, in NSTAR2000: The Physics of Excited Nucleons, pp. 255–262, arXiv:nucl-th/0004055.
[72] A. Gökalp and O. Yilmaz, The coupling constants $g_{\rho\pi\gamma}$ and $g_{\omega\pi\gamma}$ as derived from QCD sum rules, Eur. Phys. J. C **24**, 117 (2002).
[73] S. Mao, Correlations and fluctuations in a magnetized PNJL model with and without the inverse magnetic catalysis effect, Chin. Phys. C **49**, 063106 (2025).
[74] J. Mei, R. Wen, S. Mao, M. Huang, and K. Xu, Magnetic catalysis and diamagnetism from pion fluctuations, Phys. Rev. D **110**, 034024 (2024).
[75] V. Mykhaylova, M. Bluhm, K. Redlich, and C. Sasaki, Quark-flavor dependence of the shear viscosity in a quasiparticle model, Phys. Rev. D **100**, 034002 (2019).
[76] P. Chakraborty and J. I. Kapusta, Quasiparticle theory of shear and bulk viscosities of hadronic matter, Phys. Rev. C **83**, 014906 (2011).
[77] P. J. A. Bicudo, J. E. F. T. Ribeiro, and R. Fernandes, The anomalous magnetic moment of quarks, Phys. Rev. C **59**, 1107 (1999).
[78] K. Xu, J. Chao, and M. Huang, Effect of the anomalous magnetic moment of quarks on magnetized QCD matter and meson spectra, Phys. Rev. D **103**, 076015 (2021).
[79] S. Ghosh, N. Chaudhuri, P. Roy, and S. Sarkar, Thermomagnetic modification of the anomalous magnetic moment of quarks using the NJL model, Phys. Rev. D **103**, 116008 (2021).
[80] W. Thirring, Electromagnetic properties of hadrons in the static su_6 model, in *Quantum Electrodynamics*, edited by P. Urban (Springer, Vienna, 1965), pp. 205–211.
[81] G. Karl, Baryon magnetic moments and the spin of the proton, Phys. Rev. D **45**, 247 (1992).
[82] S. Capstick and B. D. Keister, Baryon magnetic moments in a relativistic quark model, arXiv:nucl-th/9611055.
[83] G. Passarino and M. J. G. Veltman, One loop corrections for e^+e^- annihilation into $\mu^+\mu^-$ in the Weinberg model, Nucl. Phys. B **160**, 151 (1979).